Investigation of Aero-Mechanical Jitter on a Hemispherical Turret

Matthew Kalensky*[a], Brian Catron[a], Stanislav Gordeyev[a], Eric J. Jumper[a], and Matthew Kemnetz[b]

[a] *University of Notre Dame, Notre Dame, IN, 46556*
[b] *U.S. Air Force Research Laboratory, Kirtland Air Force Base, New Mexico, 87117*

ABSTRACT

Optical measurements of a hemispherical turret were conducted in both a wind tunnel and airborne testing environment to measure aero-mechanical jitter imposed onto a laser beam. A hemispherical turret was positioned in the freestream flow at various protrusion distances, Mach numbers, and azimuthal angles. Lasers and accelerometers were used to quantify the mechanical contamination imposed onto the beam due to the fluid-structure interaction of the incoming freestream flow and the protruding turret body. The results from wind tunnel and in-flight testing were compared. It was shown that the wind tunnel and in-flight tests yielded different results both quantitatively and qualitatively. The possible reasons for the discrepancies between these testing campaigns were also discussed.

Keywords: Turret, wind tunnel, airborne, jitter, flight tests, aero-optical, aero-mechanical, beam control, directed energy

1. INTRODUCTION

In recent years, there has been heightened interest into the development of airborne directed energy systems. Hemispherical turrets have been identified as a geometry of interest for beam director design because of their advantageous field of regard. Consequently, the fluidic and aero-optical properties of turrets have been extensively studied both experimentally and numerically in the last decade[1-10]. The fluid mechanics around hemispherical turrets can briefly be described as follows. When subsonic flow approaches a turret body, the fluid stagnates at the lower frontal portion of the turret and creates a coherent "necklace" vortex, the "legs" of which convect downstream. The fluid that approaches the turret on the upper frontal area stagnates, and then accelerates over the top of the turret. This frontal region of the turret is fairly steady. After accelerating over the top of the turret body, separation eventually occurs. The exact location of flow separation is dependent on the state of the boundary layer near the top of the turret. Typically, however, for Reynolds numbers greater than 3×10^5, separation occurs around 120° relative to the incoming freestream[1]. After separation, a shear layer forms between the flow convecting over the top of the turret and the separated region located directly downstream of the turret. Counterrotating, symmetrical "horn" vortices form in the region directly downstream of the turret. At higher Mach numbers, this wake region becomes even more complicated. The horn vortices lose their symmetry and the formation of additional vortices originating from the back of the turret manifest[1]. It is clear that the fluidic structures downstream of the turret are complicated, highly unsteady, three-dimensional phenomena.

The aero-optical induced effects of propagating a laser through these intricate turret wake environments have been extensively studied. However, in addition to the deleterious aero-optical distortions associated with backward looking turret angles, the unsteady environment described above results in mechanical forcing imposed onto the beam director. The aero-mechanical contamination, resulting from the unsteady pressure field around the turret, can be a major source of performance degradation to these optical systems. The unsteady wake dynamics associated with the forcing on the turret can also excite mechanical modes in other optical system components such as mirrors inside the turret or on the optical bench. The aero-mechanical contamination imposed onto the laser beam manifests as tip and tilt. This results in pointing issues at the target plane, colloquially referred to as beam "jitter." Adaptive optics system components such as an optical inertial reference unit (OIRU) coupled with a fast-steering mirror (FSM), and a position sensing device (PSD) can be used in a corrective loop to alleviate the undesirable effects of mechanical corruption however, there are bandwidth limitations to these hardware components. Previous studies have been conducted that specifically target investigating the unsteady

Email | *mkalensk@nd.edu phone | (574) 631-8349

wake dynamics of turrets. In this work, the mechanical contamination imposed onto the laser beam due to the forcing on the turret is the emphasis. The authors seek to distinguish mechanical distortions associated with the unsteady forcing on the turret, excited optical system components, and facility specific distortions.

In this parametric study, a hemispherical turret is used in both wind tunnel and in-flight testing environments to measure aero-mechanical jitter as a function of Mach number, aperture angle relative to the incoming flow, and turret protrusion distances. Wind tunnel testing took place in the University of Notre Dame's Mach 0.6 White Field wind tunnel facility. In-flight testing employed the Airborne Aero-Optics Laboratory for Beam Control (AAOL-BC). The primary objective of AAOL-BC is to provide an in-flight testing platform where aero-optics experiments can be performed under real conditions[11]. AAOL-BC and predecessor programs (AAOL and AAOL-T) have been an integral part of advancing current understanding of the aero-optical interactions associated with turrets. The results of wind tunnel and in-flight campaigns are compared and relationships between test parameters and resulting aero-mechanical jitter are made.

2. EXPERIMENTAL SETUP

For convenience, Fig. 1 presents some definitions that will be used to describe the turret parameters and angles. The turret is most simply described by its aperture size, *Ap*, diameter, *D*, protrusion distance from base to apex, *H*, and cylinder height, *h*. The angle at which the beam direction is pointing can be described by the azimuthal angle, β, and the elevation angle, γ. Varying elevation angle should not drastically change mechanical jitter imposed onto the beam. Therefore, for the experiments presented in this manuscript, only an elevation angle of γ=45° was used. The turret used in the experiments presented in this work had a diameter of D=0.30 m (12 in). Additionally, a conformal turret aperture, matching the radius of curvature of the turret, is used for all tests.

2.1 Wind Tunnel Testing

Wind tunnel tests were performed at the University of Notre Dame's White Field Mach 0.6 wind tunnel facility. This facility has a 0.91 by 0.91 m (3 by 3 ft) test section capable of producing Mach numbers up to approximately 0.6. The facility is particularly useful for these experiments since the dynamic pressures in the tunnel are close to the dynamic pressures seen in real transonic flight environments. Four different protrusion distances into the freestream flow were tested: H=0.08 m (3 in), 0.15 m (6 in), 0.19 m (7.63 in), and 0.27 m (10.5 in). For protrusion distances greater than the radius of the turret, the cylindrical mount also protruded into the flow. These so called "hemisphere on cylinder" configurations have also been previously researched[1]. Figure 2 illustrates the four configurations (partial hemisphere, hemisphere, hemisphere on partial cylinder, and hemisphere on full cylinder) mounted in the wind tunnel. Notice that for the two "hemisphere on cylinder" configurations, the interface between the hemisphere and cylindrical base is covered with a plate to avoid complicated cavity flow phenomena. For all configurations, Mach numbers 0.3, 0.4, and 0.5 are tested.

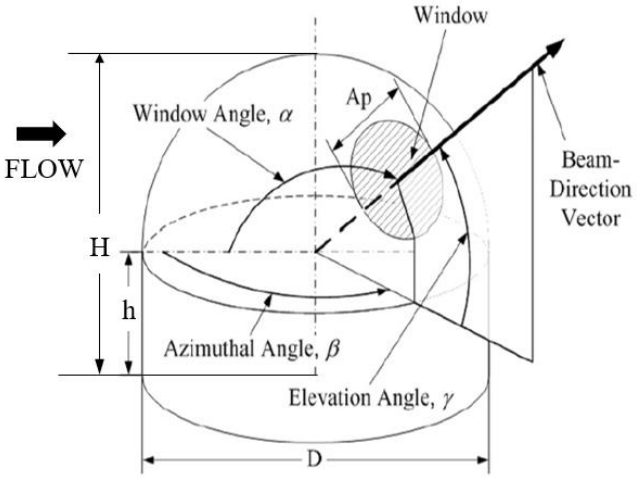

Figure 1. Turret definitions to describe parameters and angles.

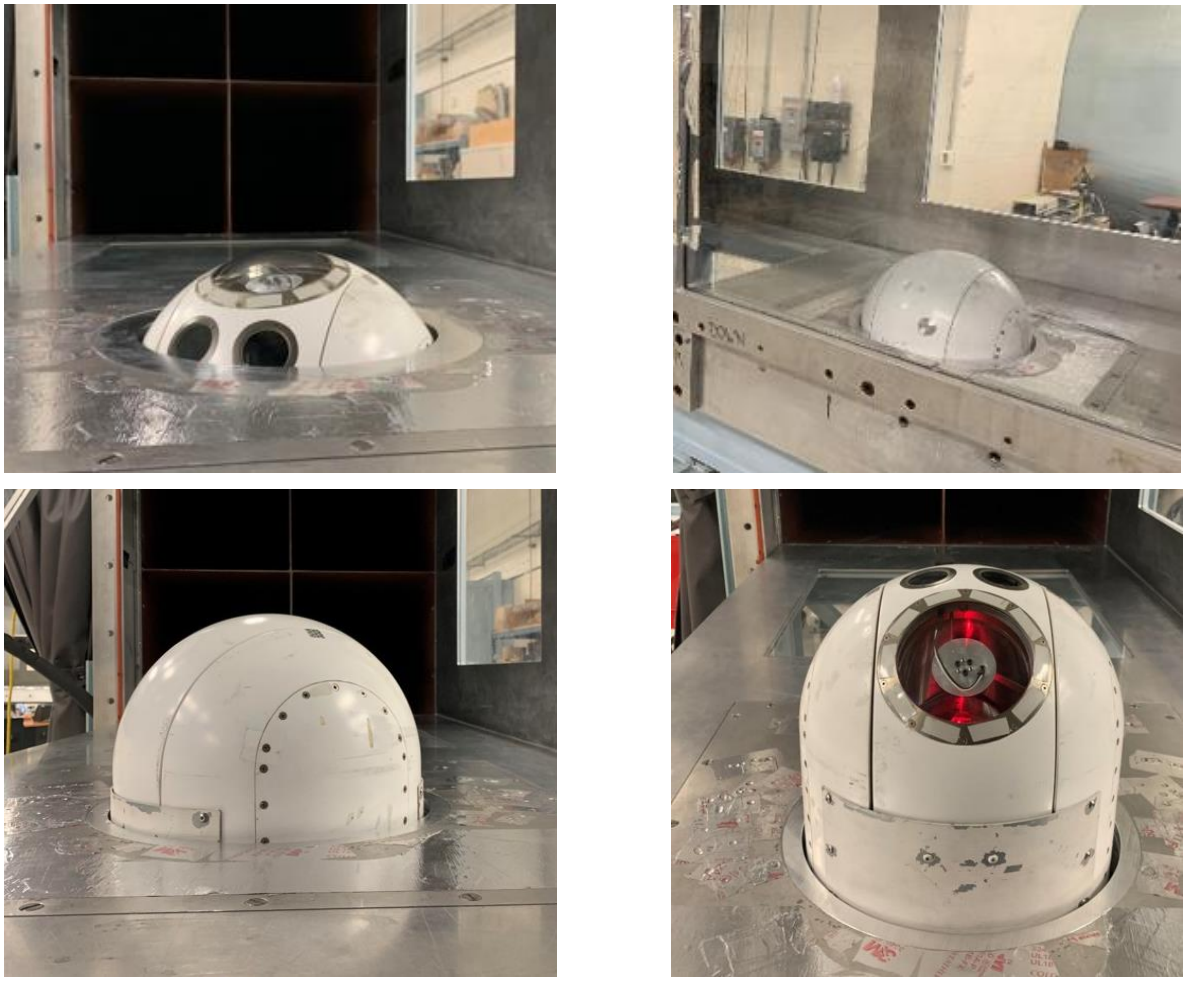

Figure 2. A) Partial hemisphere configuration. B) Hemisphere configuration. C) Hemisphere on partial cylinder configuration. D) Hemisphere on full cylinder configuration.

2.1.1 OIRU Beam

For these tests, the mechanical contamination induced jitter is measured a few ways. Firstly, an OIRU is mounted on an optical bench outside the turret. The benefit of the OIRU is that the outputted beam is inertially stabilized, meaning any bench or lab vibrations up to a certain bandwidth are rejected from the outgoing beam. The OIRU beam passes through a 50/50 beam splitter and then enters the turret parallel to the optical axis of the system. Rather than exiting the turret through the viewing aperture, the OIRU beam is reflected off a mirror installed on the back of the secondary mirror of the telescope. As such, the return beam then follows the same path back out of the turret. The beam is turned by the same 50/50 beam splitter and is then focused by a 250 mm lens onto a Phantom v1611 high speed camera. The camera collected images at 30 kHz for 30 seconds with a spatial resolution of 128 by 128 pixels each 28 μm in height and width. By knowing the focal length of the last lens and the pixel size of the camera, a centroid can be extracted in order to compute *x*-, *y*-, and subsequently radial jitter as a function of time. For each Mach number and turret configuration, azimuthal angles β=0, 30, 60, 75, 90, 105, 120, and 150° relative to the incoming freestream were also tested. Figure 3 shows the optical setup for these measurements outside the turret.

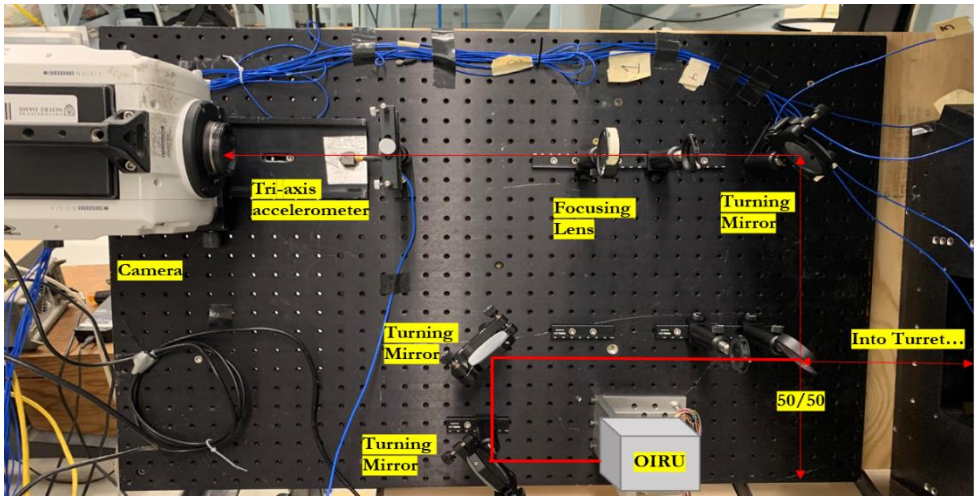

Figure 3. Optical setup for the OIRU beam outside of the wind tunnel and turret.

2.1.2 Reflector Mounted Laser Diode

The second method of data collection is by using a blue laser diode installed in the reflector mirror mounted on the back of the secondary mirror (the same mirror the OIRU beam is reflected off). A close-up of this reflector mirror can be seen in Fig. 4. Despite this beam not being inertially stabilized like the OIRU beam, the jitter measurements collected using the blue laser diode only pass through the optical path of the turret once. For these measurements using the reflector mounted laser diode, the camera collected images at 20 kHz for 12 seconds with a spatial resolution of 256 by 256 pixels. These measurements are compared with the jitter imposed onto the OIRU source. Again, for each Mach number and turret configuration, azimuthal angles β=0, 30, 60, 75, 90, 105, 120, and 150° relative to the incoming freestream were also tested. The optical bench setup outside the turret for the blue laser diode can be seen in Fig. 5.

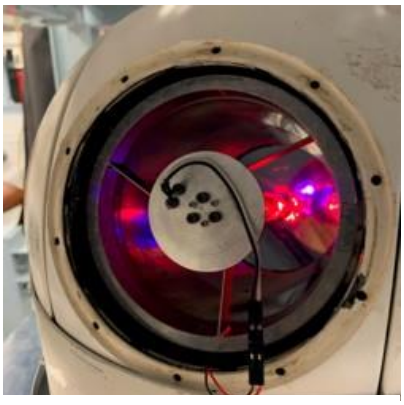
Figure 4. Reflector mounted on the back of the secondary mirror inside the turret telescope.

2.1.3 Bench Measurements

In addition to the measurements involving the OIRU beam and the reflector mounted laser diode, bench measurements were also collected. For these bench measurements, the OIRU beam was used and turned towards the camera before entering the turret. The jitter that was imposed onto this beam was from optical components that were exclusively on the optical bench. These measurements gave a baseline estimate of what jitter comes from the optical bench vibration versus the aero-mechanical forcing on the turret itself. Azimuthal angles of β=0, 90, and 150° were tested for these bench measurements.

2.1.4 Accelerometer Measurements

For all the measurements described above (OIRU beam, reflector mounted laser diode, and bench measurements), simultaneous accelerometer measurements were also recorded. For these tests, 6 accelerometers were used: 1 tri-axis and 5 single axis. The tri-axis accelerometer was placed on the mounting bracket of the high-speed camera used to collect jitter measurements, as seen in Figs. 3 and 5. Three single axis accelerometers were placed in directions pointing with respect to x, y, and z on the turret collar which presses up against the wind tunnel. The last two accelerometers were placed on the mounting stands for two turning mirrors located inside the turret. Accelerometers were sampled at 30 kHz for the OIRU beam and bench measurements and then 20 kHz for the reflector mounted laser diode measurements. All accelerometers were collected simultaneous to the high-speed camera. The voltage measurements collected using the accelerometers are converted to accelerations using company provided calibrations. Accelerations are then converted to displacements by using a simple midpoint rule twice.

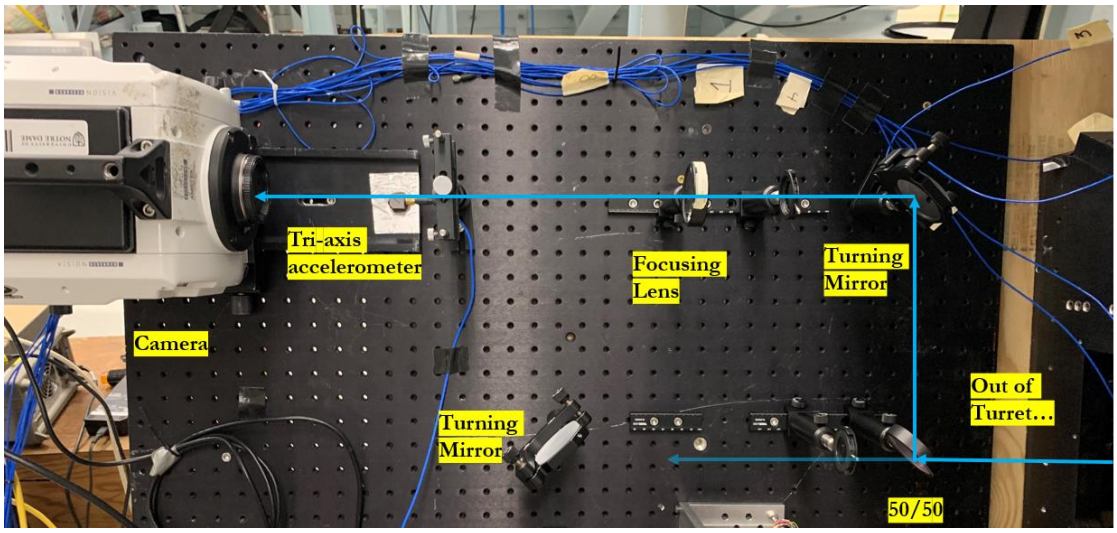

Figure 5. Optical setup for the blue laser diode outside of the wind tunnel and turret.

2.2 AAOL-BC Testing

AAOL-BC is an airborne laboratory, retrofitted to accommodate equipment to perform optical experiments[11-14]. For these tests, the same turret used for wind tunnel tests and described above was installed in the aircraft. Two flights campaigns were conducted where the turret was flown in the "hemisphere" and "hemisphere on full cylinder" configurations. Figure 6 shows the two turret configurations mounted in the aircraft. Similar to the wind tunnel tests, two laser sources were used to measure the aero-mechanical imposed jitter. Instead of using the OIRU for these flights tests, a 532 nm continuous laser was used and rigidly mounted to the optical bench in the aircraft. An OIRU was not used since the pitch, yaw, and roll of the aircraft exceeds the rejection capability of the unit. There was consideration for an inertial feedback loop to the OIRU but in that case, the measuring device would also need a stabilization platform. Ultimately, the assumption was made that the jitter contribution associated with using a non-stabilized platform is much smaller than the jitter imposed onto the beam due to the aero-mechanical forcing on the turret, which is why the 532 nm continuous laser was used. The same reflector mounted laser diode that was used during the wind tunnel tests was also used for these flight campaigns. Instead now, a kinematic mount was designed and implemented to give the reflector mounted laser diode its own steering capability separate from the mounting of the reflector itself. This mount can be seen in Fig. 7. The utility of this approach is that it allows for both beams to be scored onto the camera simultaneously. Therefore, for these flight tests, the rigidly mounted 532 nm continuous laser, the reflector mounted laser diode, and the accelerometers were all collected simultaneously.

Figure 6. A) Hemisphere configuration mounted in AAOL-BC aircraft. B) Hemisphere on full cylinder configuration mounted on AAOL-BC aircraft.

Figure 8a shows the inside of the aircraft with the equipment and turret installed. Figure 8b shows the optical setup used on the inside of the aircraft. The camera collected images at 30 kHz for 30 seconds with a spatial resolution of 128 by 128 pixels. For both the hemisphere and the hemisphere on full cylinder configurations, Mach numbers 0.3, 0.4, 0.5, and 0.6 were tested as well as azimuthal angles $\beta = 60$, 75, 90, 105, 120, and 150°. Mach numbers 0.3, 0.4, and 0.5 were tested at 3,050 m (~10,000 ft) and Mach numbers 0.5 and 0.6 were tested at 6,700 m (~22,000 ft). Mach 0.5 measurements were collected at both altitudes to have overlap in data at the same Mach number but different dynamic pressures. As mentioned above, simultaneous accelerometer measurements were also collected. For these flight tests, 10 accelerometers were used (1 tri-axis and 9 single axis). The tri-axis accelerometer was mounted on the camera mounting bracket. Two single axis accelerometers were mounted on the laser mounting platform. Two single axis accelerometers were mounted in the turret on the mounting mechanisms for the two turning mirrors in the same locations as the wind tunnel experiments. One accelerometer was placed in the middle of the optical bench. Two accelerometers were placed on the top and side of where the turret collar presses up to the aircraft door and two were placed on the top and side of the turret collar itself. All accelerometers were sampled at 60 kHz for the full duration of camera measurements.

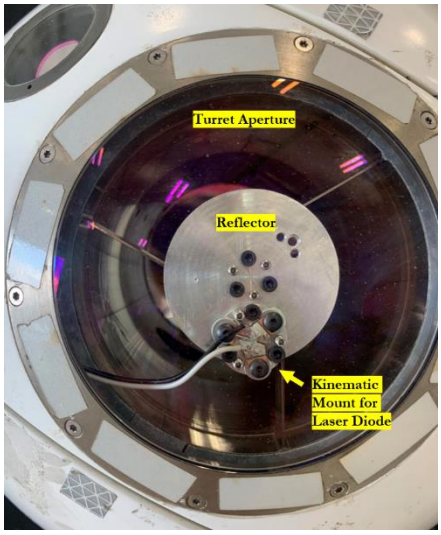

Figure 7. Kinematic mount for laser diode attached to reflector.

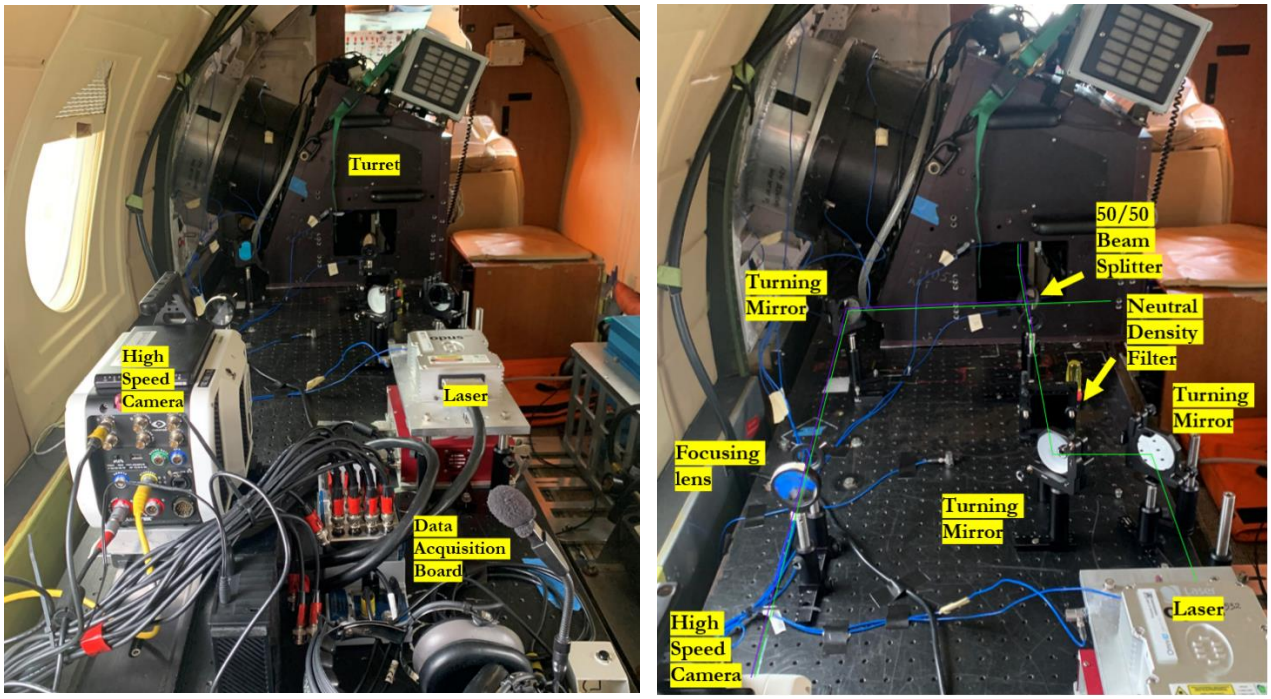

Figure 8. A) Inside of AAOL-BC aircraft with experiment hardware. B) Optical setup inside AAOL-BC aircraft.

3. DATA REDUCTION AND ANALYSIS

A simple centroiding algorithm, such as a first moment scheme, works great for an image with a single measurement beam on the camera like the wind-tunnel testing data had. However, when multiple beams are present, as was the case with the AAOL-BC flight data, other approaches need to be taken. In order to handle multiple beams, a MATLAB function called "regionprops" was employed. This function starts by looking at the mask of pixels that exceed a user defined intensity threshold. Then, the algorithm determines regions of associated pixels. Once a relevant set of regions is determined, the function looks at the pixel values in that region and computes a centroid based on the first moment method. Additional statistics such as spot major and minor dimensions, orientation, equivalent diameter, and the mean and max intensity were recorded to track a given beam throughout the time series. In order to have the capability of handling intermittent image noise, a mean image was computed and run through the same function to determine the general area that each beam encompasses. For each frame, the beam that was closest to a mean beam location and within some user defined minimum distance, was assigned to that beam's data array. This ensures that the same beam is constantly referenced throughout the test point.

Once the camera images are converted into usable data by extracting a centroid of the beams in each frame, knowing the pixel size and focal length of the focusing lens allows the x- and y-jitter imposed onto the beam to be extracted as a function of time. Even though looking at specific x- and y-jitter time series has its benefits, the x- and y-jitter time series are often converted into a radial, or total jitter time series using Eq. 1.

$$\sigma_T(t) = \sqrt{\sigma_x^2(t) + \sigma_y^2(t)} \tag{1}$$

4. RESULTS AND DISCUSSION

4.1 Wind Tunnel Test Results

Wind tunnel test results for radial jitter imposed onto the beams are presented in Fig. 9. Each plot represents a different Mach number test case and the rms radial jitter is plotted as a function of azimuthal angle for each turret geometry. The left plots present the results for jitter measured using the OIRU configuration while the right plots present the results using the reflector mounted blue laser diode. Here it can be seen that increasing the freestream Mach number results in more jitter imposed onto the laser beam for all configurations. More jitter was consistently measured on the OIRU beam than the reflector mounted blue laser diode beam because the OIRU beam experiences a double pass through the turret's optical path. In many instances, the jitter imposed onto both beams was higher for the cases of greater turret protrusion. However, the resultant jitter is clearly heavily dependent on many factors besides turret protrusion. The partial hemisphere produced significantly less jitter than the other configurations for most azimuthal angles while the hemisphere on full cylinder configuration typically produced the most beam jitter for most azimuthal angles.

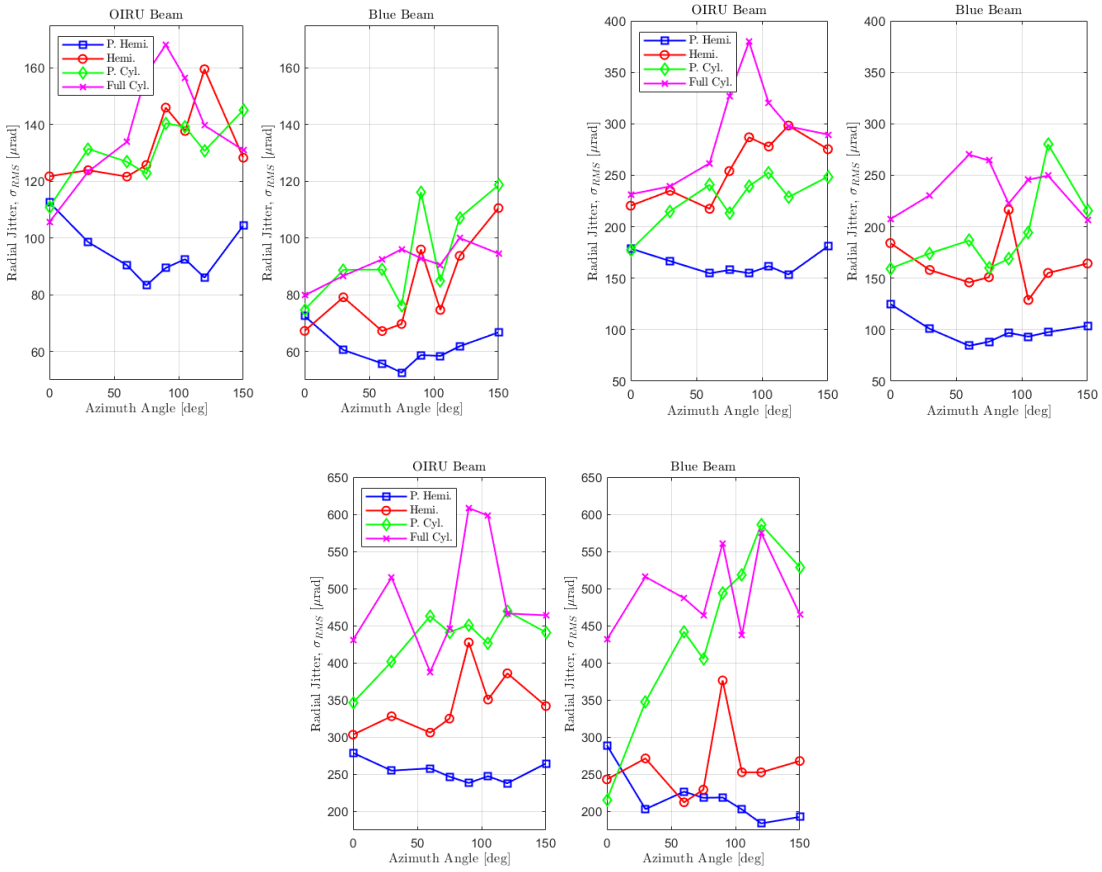

Figure 9. Comparison of resultant radial jitter for all four turret configurations. A) Freestream Mach number of 0.3. B) Freestream Mach number of 0.4. C) Freestream Mach number of 0.5.

Varying the azimuthal angle of the turret also caused variations in the amount of jitter imposed onto the beam, with azimuthal angles around 90 degrees typically causing the most jitter and the forward-looking angle of 0 degrees producing the least jitter. The internal architecture of the turret is not symmetric around the turret. Therefore, by varying azimuthal angle, the center of gravity of the turret as well as where the optical components are located changes.

Another visualization of the jitter test results is presented in Fig. 10. Here, each plot corresponds to a different configuration. The measured jitter imposed onto the OIRU beam, the reflector mounted blue laser diode beam, and the bench measurements are plotted as a function of azimuthal angle. All plots within this figure correspond to measurements taken at a freestream Mach number of 0.5. Variations of resultant measured jitter from the OIRU beam and the reflector

mounted blue laser diode as a result of changing azimuthal angle are still apparent in this alternate representation. Also plotted are the bench measurements made by turning the OIRU beam before entering the turret. These "bench measurements" record the jitter imposed onto the beam from only components on the optical bench, and not any mechanical contamination associated with the vibrating internal components of the turret. However, the measured contamination associated with the bench measurements may still be related to aero-mechanical forcing due the interconnected mounting of the bench, turret, and wind tunnel. It can be seen that the resultant jitter from just the bench measurements is substantial. In fact, in some extreme scenarios such as the partial cylinder case at an azimuthal angle of 0 degrees, the bench measurements alone produced more jitter than the jitter measured by the reflector mounted blue laser diode single pass measurement. Furthermore, the bench measurements do also have a slight dependence on azimuthal angle. This reveals that the way the bench, turret, and wind tunnel facility are mounted together, creates common mechanical contamination across the entire experimental setup.

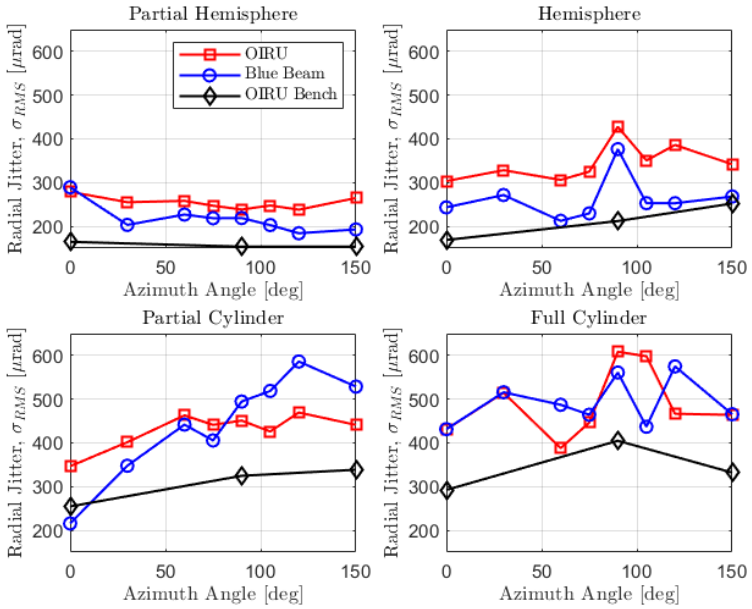

Figure 10. Comparison of resultant radial jitter for different measurement methods at Mach 0.5. A) Partial hemisphere measurements. B) Hemisphere measurements. C) Hemisphere on partial cylinder measurements. D) Hemisphere on full cylinder measurements.

This result makes it difficult to make concrete research assertions from strictly looking at the rms radial jitter results. The contamination imposed onto the laser beam is a function of many factors however some of which are specific to the architecture of this turret as well as the facility the system is being tested in. The goals of this research are to identify characteristics which are consistent between facilities and different turret designs, such as Mach number and geometry effects. To accomplish this, the spectra and accelerometer measurements are also be analyzed.

Figure 11 presents power spectral density (PSD) results for the jitter measured on the hemispherical configuration in the 90-degree azimuthal angle position. The three left plots are the PSDs of the x-jitter, and the three right plots are the PSDs of the y-jitter. Results from all Mach number cases are also plotted. On the plots themselves, red represents the spectra from the OIRU measurements, blue represents the spectra from the reflector mounted blue laser diode measurements, and black represents the spectra for the bench measurements. In these results, it is immediately obvious that jitter associated with the bench comes from almost entirely low frequency vibrations with most of the energy at frequencies less than 900 Hz. Very low frequency peaks, such as at approximately 15-20 and 35-40 Hz for example are apparent in all measurements. Since the turret is rigidly mounted to the optical bench, which is rigidly mounted to the wind tunnel, it is difficult to determine which frequencies are associated with aero-mechanical forcing versus facility corruption. Unfortunately, in addition to being hard to distinguish, a coupling between these different experimental features also exists which makes isolating the jitter contribution associated with specifically aero-mechanical forcing difficult. Despite the lower frequency content being harder to distinguish the origins of the vibrations, at higher frequencies (greater than 900 Hz) almost no jitter

comes from the optical bench components. This is expected as at some point, the optical bench will attenuate higher frequencies and act as a low pass filter. Therefore, these higher frequencies are associated with strictly the internal components of the turret. Two notable spectral peaks are at approximately 1 and 2.4 kHz. Neither of these spectral peaks are apparent in the bench measurements however are very prominent in the spectra for the OIRU measurements as well as the reflector mounted laser diode measurements. Between 650 and 750 Hz, there is also a large spike in the spectral content for both the OIRU beam as well as the reflector mounted laser diode beam while the bench measurements show relatively low spectral energy at this frequency. It is likely that these three spectral regions are likely associated with different excited vibrational modes of optical components within the turret itself as they do not shift in frequency with increasing Mach number.

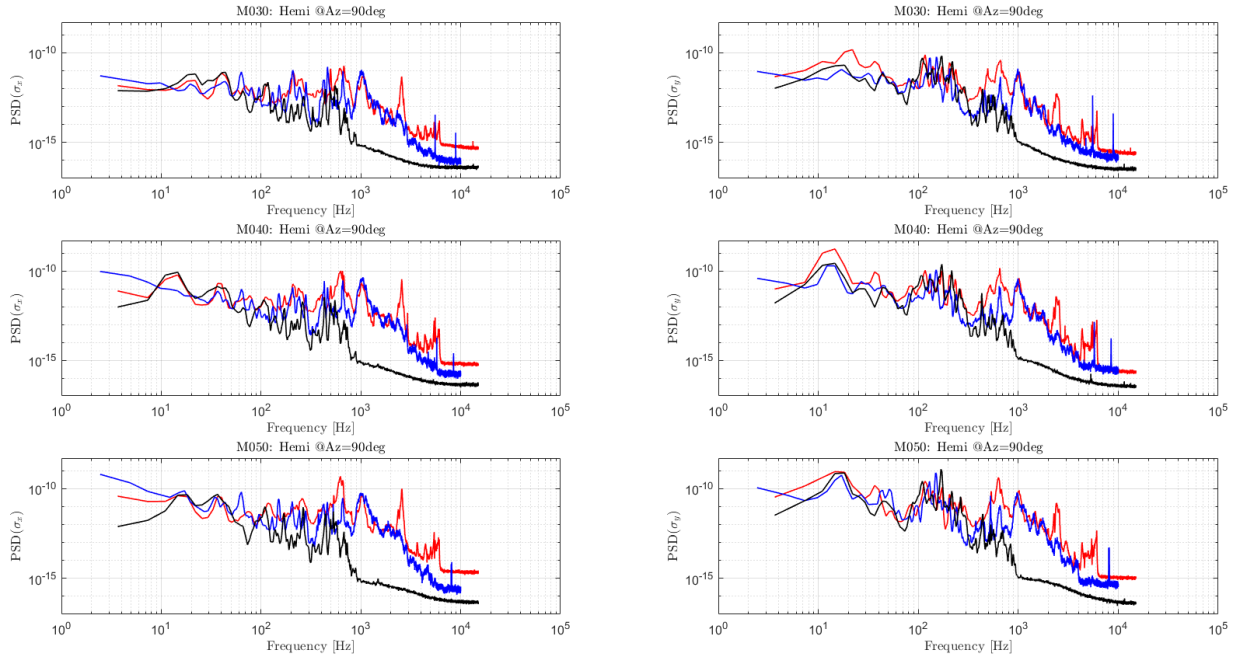

Figure 11. Power spectral density plots for x- and y-jitter at all Mach numbers for the hemisphere configuration at an azimuthal angle of 90 degrees.

Figure 12 presents the PSD results for the x-jitter measured from the OIRU beam for all configurations at Mach 0.3 (left plot) and Mach 0.5 (right plot) at an azimuthal angle of 90 degrees. These results are plotted as a function of Strouhal number, $St_D = fD/U_\infty$, where D is the turret diameter and U_∞ is the freestream velocity. Previous studies have found that there are two major modes in the wake dynamics of a turret: antisymmetric, or alternate shedding of vortices off the back of a turret and symmetric vortex shedding. The antisymmetric, unsteady vortex shedding occurs in the normalized frequency range of, $St_D = 0.15 – 0.2$. Emphasized by a red dotted boxes in the left and right plots of Fig. 12, are pronounced peaks located at $St_D = 0.19$. It is believed that these spectral peaks are associated with mechanical contamination due to the unsteady forcing caused by antisymmetric vortex shedding. This is further validated by the increasing energy associated with this spectral peak as a function of turret protrusion into the freestream flow. For the case of the partial hemisphere, the turret is only barely sticking into the flow. Therefore, the wake dynamics for the partial hemisphere case are dominated by symmetric vortex shedding and the unsteady, spanwise anti-symmetric forcing on the turret is minimal. Consequently, for the case of the partial hemisphere, the spectral peak at St_D=0.19 is small. On the other hand, for greater turret protrusion into the flow, such as the case of the hemisphere on full cylinder, the peak at St_D=0.19 becomes large and it is believed that the dynamics of the wake are dominated by unsteady, alternate vortex shedding. The well documented Strouhal range of 0.15-0.2 for wake dynamics of a hemispherical turret originated from investigating the fluid mechanics of the wake. This does not necessarily mean that the vibrational response of the system should demonstrate the same spectral phenomena however, a peak at St_D=0.19, is noticed here in the wind tunnel test results and is consistent across the varying Mach numbers.

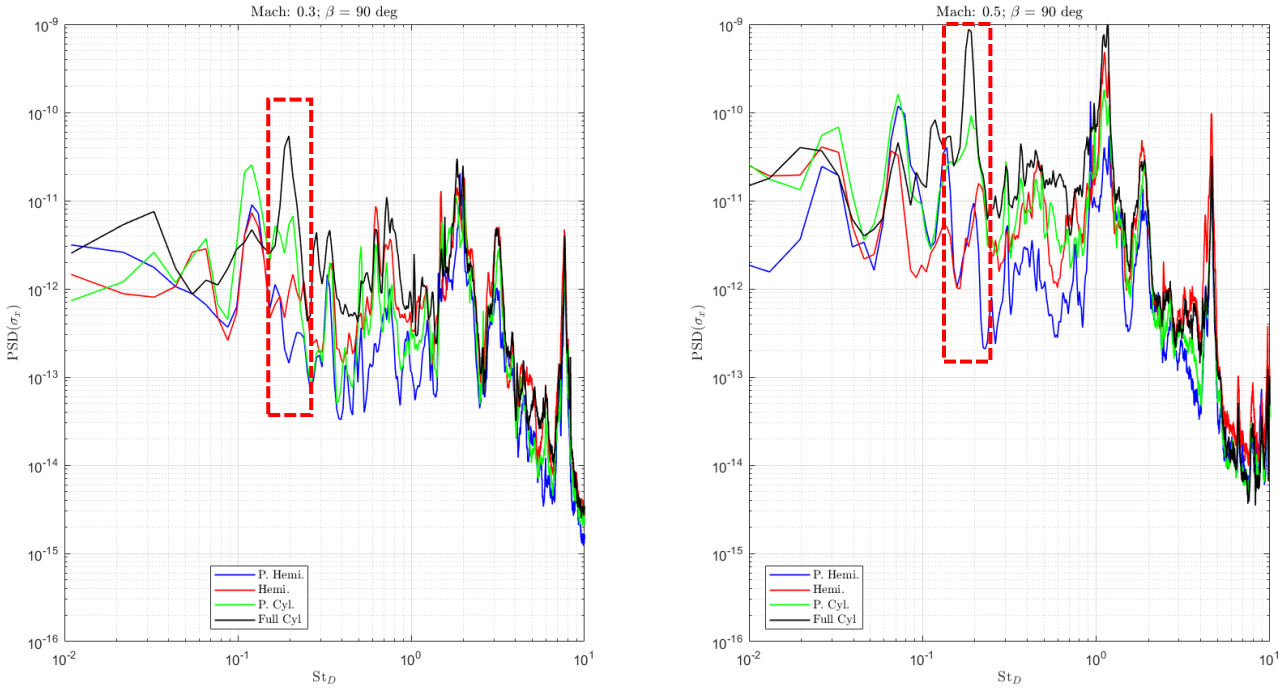

Figure 12. Power spectral density plots of x-jitter measured from the OIRU beam for all configurations at an azimuthal angle of 90 degrees and Mach number of 0.3 (left plot) and 0.5 (right plot).

Accelerometer measurements were also collected during the wind tunnel experiments. Although six accelerometers were used, the results associated with the two accelerometers attached to the turret mounting ring are going to be the emphasis of the following analysis. The locations of these accelerometers can be seen in Fig. 13. Pre-multiplied power spectrums were calculated for the displacement vectors calculated from these accelerometer measurements for the Mach 0.3 and 0.5 cases, at an azimuthal angle of 90 degrees, and for both the hemisphere and hemisphere on full cylinder configurations. The utility of the pre-multiplied spectra is that it allows one to visually identify the highest contributing energetic frequencies. These results can be seen in Fig. 14. Here, the blue line represents the spectrum for the hemisphere on full cylinder and the red line represents the spectrum for the hemisphere configuration. The left plots correspond to the Mach 0.3 cases and the right plots correspond to the Mach 0.5 cases. Additionally, the top plots correspond to the spectra from measurements collected by the streamwise accelerometer while the bottom plots correspond to the spectra calculated from the spanwise mounted accelerometer. Here it can be seen that in the streamwise direction, the hemisphere configuration produces more mechanical contamination which also significantly increases with Mach number. Peaks in the spectra exist between 650 and 800 Hz and at 1 kHz similar to the spectra of the beam jitter shown in Fig. 11. In the spanwise direction, the hemisphere on full cylinder configuration produces more mechanical contamination which also increases with Mach number.

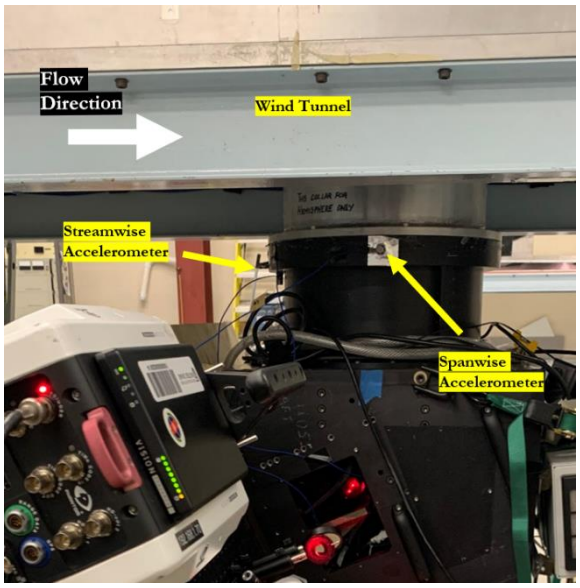

Figure 13. Streamwise and spanwise accelerometer locations attached to turret mounting ring.

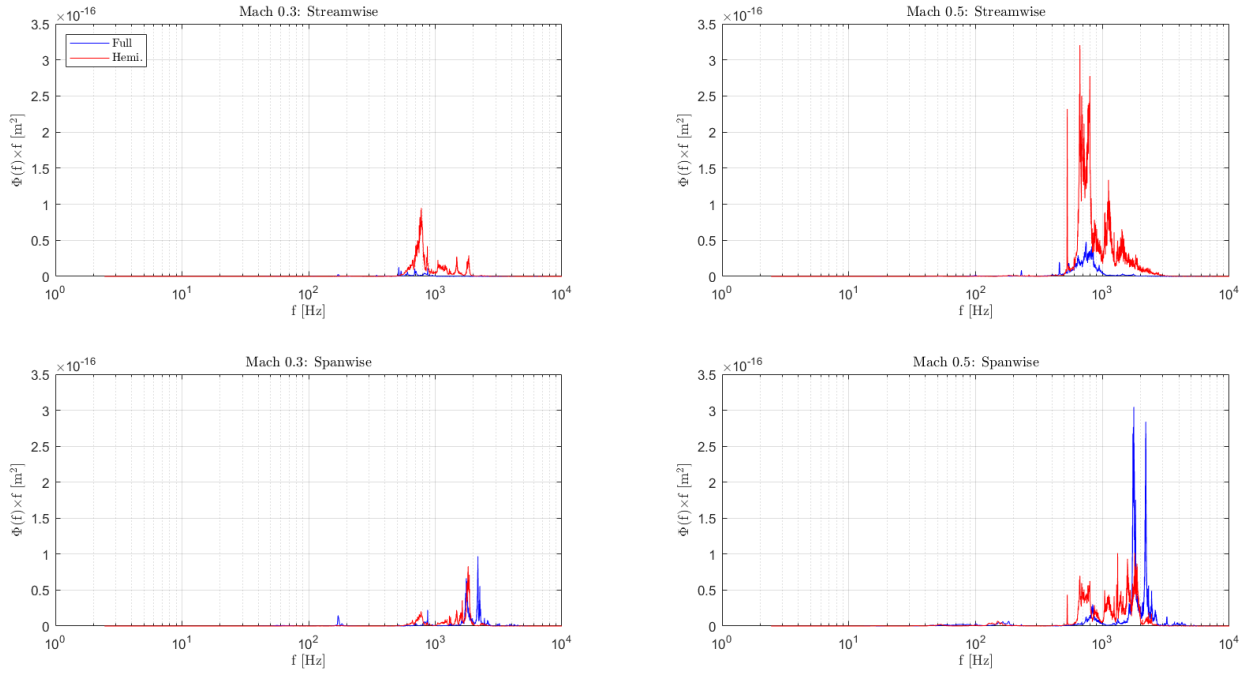

Figure 14. Pre-multiplied power spectral densities of displacement measurements for the hemisphere and hemisphere on full cylinder configurations at an azimuthal angle of 90 degrees. A) The case of Mach 0.3 for the streamwise accelerometer. B) The case of Mach 0.5 for the streamwise accelerometer. C) The case of Mach 0.3 for the spanwise accelerometer. D) The case of Mach 0.5 for the spanwise accelerometer.

4.2 AAOL-BC Test Results

Jitter measurements were also collected using AAOL-BC. Figures 15 and 16 present radial jitter results measured on the optical bench mounted green beam as well as the reflector mounted blue laser diode beam for the hemisphere and hemisphere on full cylinder configurations, respectively. As mentioned above, the Mach 0.5 measurements were collected at an altitude of approximately 3050 m (~10,000 ft) as well as 6700 m (~22,000 ft) to have measurement overlap for

different dynamic pressures. When the green optical bench laser measurements are divided by two to account for the double pass, the two types of jitter measurements are in agreement with each other. Changing azimuthal angle also very minimally changes the resultant jitter imposed onto the beam. Figure 17 compares the jitter results from the reflector mounted laser diode source for both the hemispherical and hemisphere on full cylinder configurations at all tested Mach numbers. Interestingly, the jitter imposed onto the beam for the two different configurations are very similar across all Mach numbers.

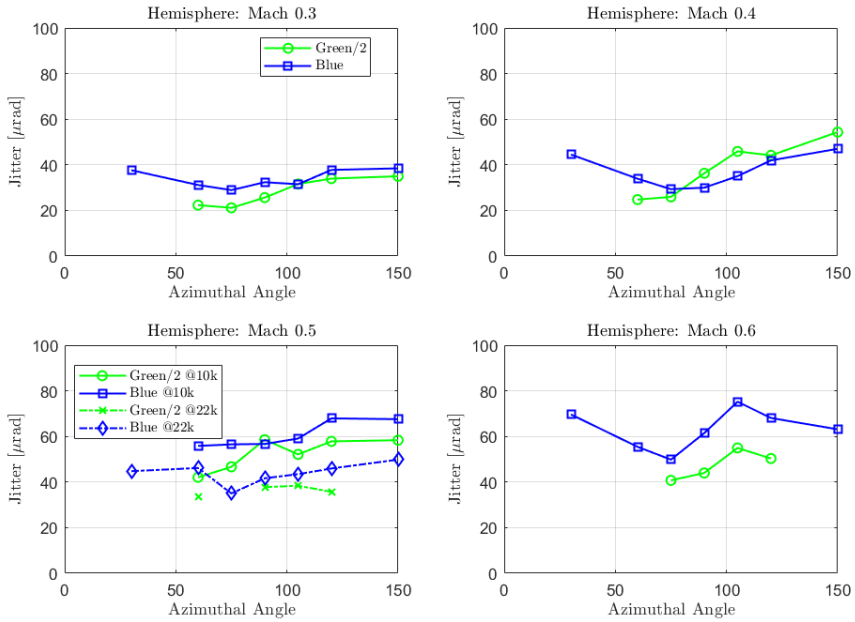

Figure 15. Radial rms jitter results from both the optical bench mounted green beam as well as the reflector mounted blue laser diode beam for the hemisphere configuration. All tested azimuthal angles are presented as well as Mach numbers A) 0.3 B) 0.4 C) 0.5 and D) 0.6.

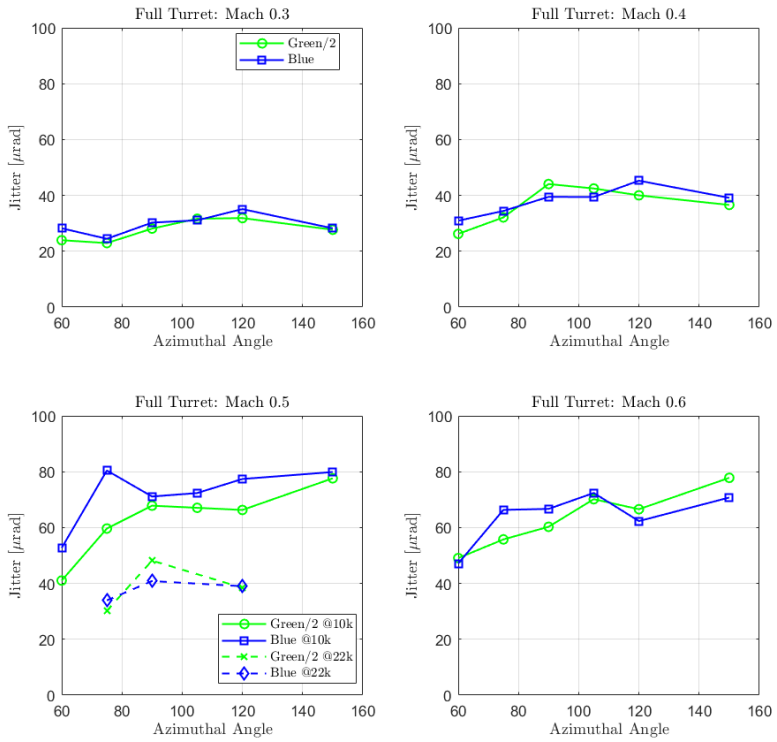

Figure 16. Radial rms jitter results from both the optical bench mounted green beam as well as the reflector mounted blue laser diode beam for the hemisphere on full cylinder configuration. All tested azimuthal angles are presented as well as Mach numbers A) 0.3 B) 0.4 C) 0.5 and D) 0.6.

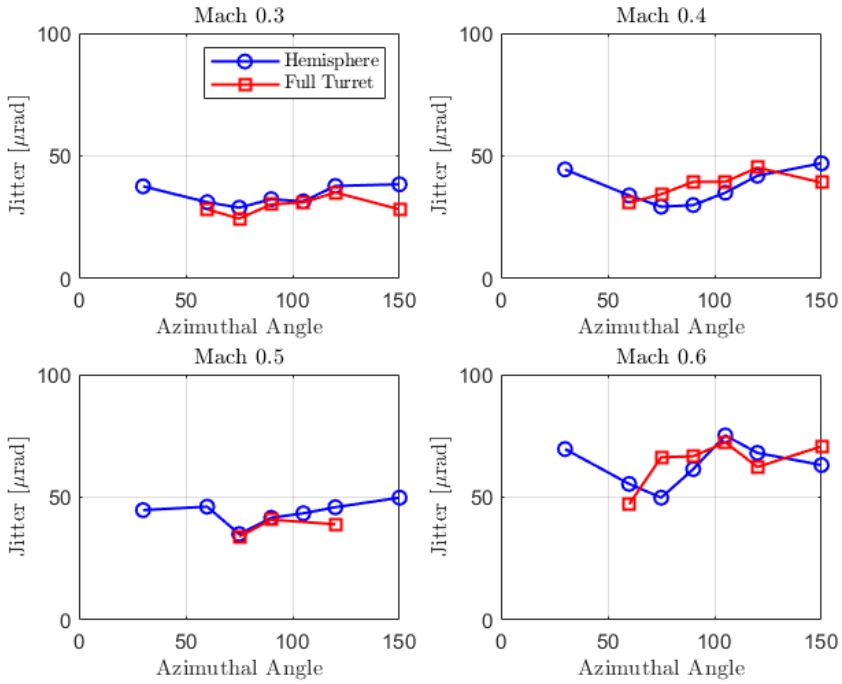

Figure 17. Radial rms jitter plots from the reflector mounted blue laser diode measurements for both the hemisphere and hemisphere on cylinder results. All azimuthal angles are presented as well as Mach numbers A) 0.3 B) 0.4 C) 0.5 and D) 0.6.

Figure 18 presents the power spectral density calculated from the reflector mounted laser diode measurements for both the hemisphere as well as the hemisphere on full cylinder configurations at Mach 0.3 and 0.5 and an azimuthal angle of 90 degrees. Here it can be seen that, similar to the wind tunnel spectra, high energy spectral peaks exist at around 1 kHz and between 650-750 Hz.

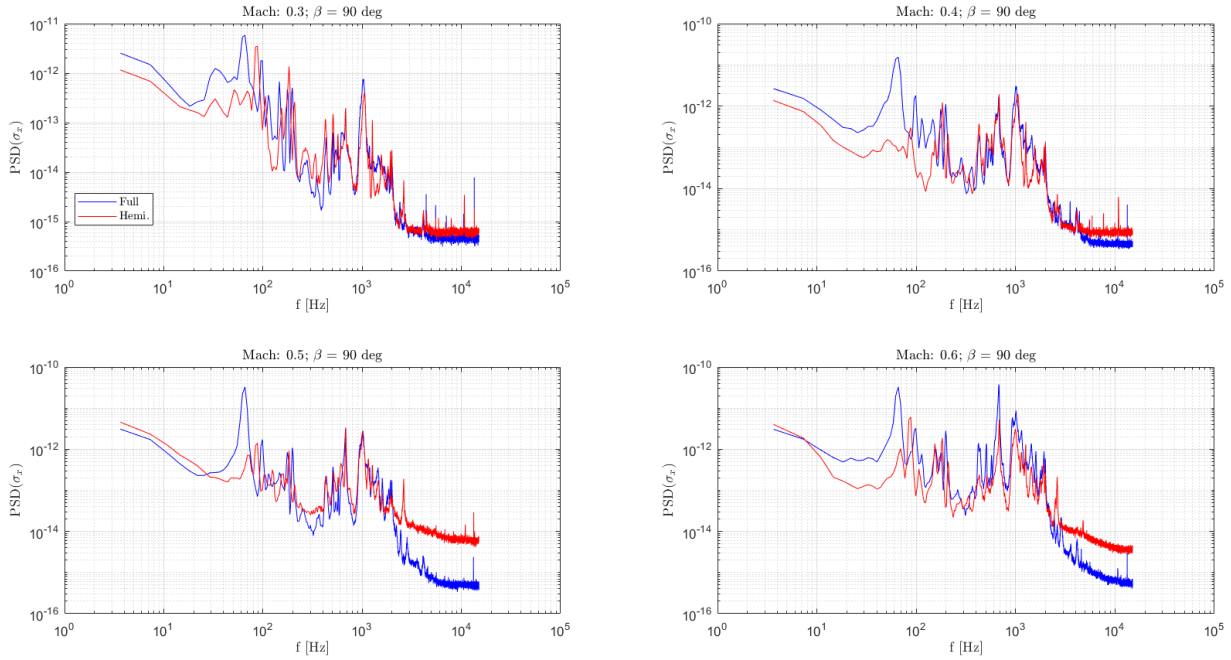

Figure 18. Power spectral density plots of x-jitter measured from the reflector mounted blue beam for the hemisphere and hemisphere on full cylinder configurations at an azimuthal angle of 90 degrees and Mach numbers A) 0.3 B) 0.4 C) 0.5 and D) 0.6.

Accelerometer measurements were also collected during the AAOL-BC tests. The analysis presented below will focus on the accelerometer measurements collected on the aircraft door above and to the side of where the turret mounts. The locations of these accelerometer measurements can be seen in Fig. 19. Same as for the wind tunnel tests, pre-multiplied power spectrums were again calculated for the displacement vectors calculated from these accelerometer measurements for the Mach 0.3 and 0.5 cases, at an azimuthal angle of 90 degrees, and for both the hemisphere and hemisphere on full cylinder configurations. The results can be seen in Fig. 20. Recall, the accelerometers were sampled three times as fast during flight testing compared to the wind tunnel testing. Therefore, the resulting spectrum spans a wider range of frequencies. It can be seen that a range of frequencies between 800 to 1200 Hz were particularly energetic which is in agreement with the jitter spectrum results plotted in Fig. 18. The hemisphere on full cylinder case very clearly created more mechanical contamination as measured by the two door mounted accelerometers compared to the hemisphere configuration.

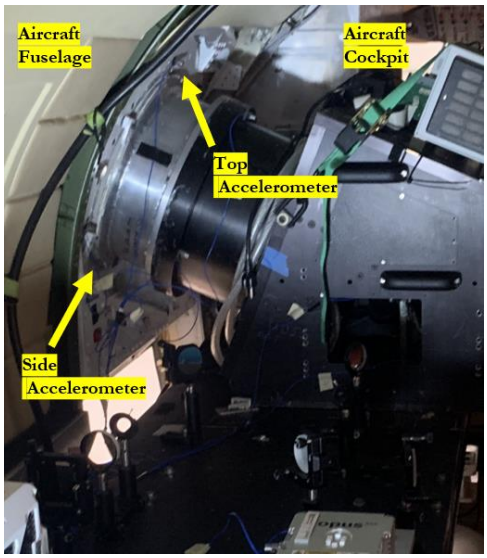

Figure 19. Accelerometer locations in AAOL-BC aircraft.

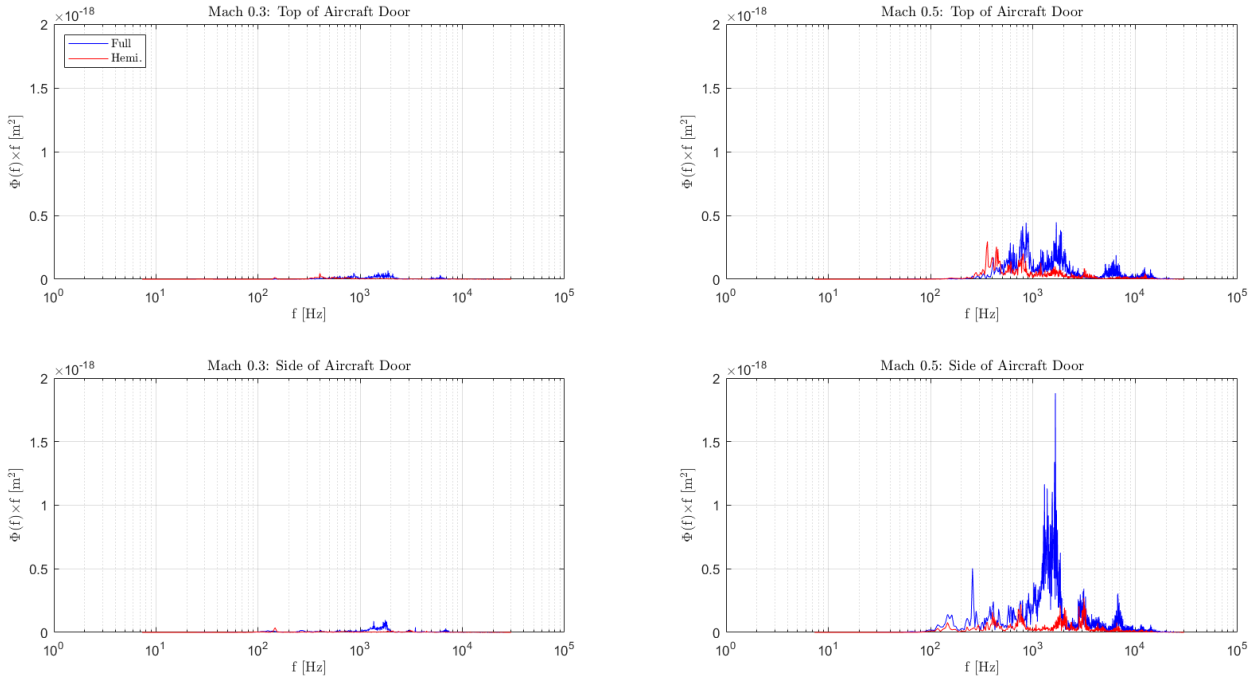

Figure 20. Pre-multiplied power spectral densities of displacement measurements for the hemisphere and hemisphere on full cylinder configurations during in-flight testing at an azimuthal angle of 90 degrees. A) The case of Mach 0.3 for the streamwise accelerometer. B) The case of Mach 0.5 for the streamwise accelerometer. C) The case of Mach 0.3 for the spanwise accelerometer. D) The case of Mach 0.5 for the spanwise accelerometer.

4.3 Comparison Between Wind Tunnel and AAOL-BC Test Results

The differences in findings between the wind tunnel tests and the in-flight tests are counterintuitive but not unreasonable. Despite best efforts to keep setups similar between wind tunnel and flight tests, the nature of these experiments is that the measured jitter is inherently susceptible to any differences in experimental apparatuses. Fundamentally, the differences in turret mounting, the base motion of the aircraft, and the difference between being within a wind tunnel facility and aircraft all introduce differences in setup that vibrational modes of system hardware are sensitive to.

Resultant rms radial jitter from both wind tunnel and in-flight testing did increase with Mach number. However, no noticeable scaling patterns were observed. It is believed that vibrational amplitude should scale with dynamic pressure. This was not noticed from either lab testing or in-flight testing results. The reason for this is likely because the experimental components subjected to a varying dynamic pressure only contributed to a portion of the overall resultant jitter. The modes and frequencies which may scale with increasing Mach number were simply washed out by other contaminating sources.

For both the jitter and accelerometer measurements, the distortions associated with lab testing were much greater than in-flight testing. More interesting than the quantitative differences between wind tunnel and in-flight testing are the qualitative differences in the resultant jitter. The wind tunnel test results demonstrated an increase in jitter imposed onto the beam with increasing turret protrusion distance. Although only two configurations were tested for the in-flight campaigns, this trend was not observed. In fact, the resulting rms radial jitter results during the in-flight tests were remarkably similar between the hemisphere and hemisphere on full cylinder configurations. This may be an indication that the increase in jitter with protrusion distance noticed during the wind tunnel tests may be associated with vibrations caused by increased tunnel blockage. The wind tunnel tests also showed more variation in resultant jitter when changing azimuthal angle. This is likely associated with the rigid mounting between the wind tunnel, turret, and optical bench. When the center of gravity of the turret changes due to a change in azimuthal angle in the wind tunnel facility, this change is felt by the entire experimental setup. This is reflected in the wind tunnel bench measurements where changing azimuthal angle changed the resultant jitter for when the beam only encountered optical bench components. In the aircraft, the turret is rigidly mounted to the aircraft door, however the plane itself has no opposite force acting on it. Therefore, forces acting on the turret and subsequently on the aircraft are likely dampened out. For the in-flight campaigns, very small differences in resultant rms jitter were noticed between different azimuthal angles.

The power spectrum results for jitter calculated from the wind tunnel testing revealed a prominent peak at St_D=0.19. It is believed that this peak is associated with the unsteady vortex shedding downstream of the turret. During the in-flight testing, no such peak was observed. It is possible that the existence of the wind tunnel walls serves to amplify these wake dynamics and for obvious reasons, this does not happen in-flight. Another possibility for the absence of this peak in the flight test results has to again do with the mounting mechanisms for the wind tunnel and in-flight testing. It is well documented that St_D=0.15 – 0.20 is the expected normalized frequency range for the unsteady vortex shedding downstream of the turret. However, for these tests, pressure was not measured. It may be possible that the unsteady pressure between St_D=0.15 – 0.20 manifests as St_D=0.19 in optical contamination for the wind tunnel tests but not the flight testing. The unsteady pressure field can cause certain vibrational modes but not necessarily at the frequency associated with the pressure field.

This point begins to express the difficulties associated with these experiments. Studying the origins and factors causing mechanical contamination imposed onto the laser beam will require meticulous investigation into the vibrational properties of every system component as well as detailed finite element analysis. Once all the system components vibrational properties and responses are known, the resultant "optical signature" associated with these vibrations should be modeled. Subsequently, experiment testing should be conducted but in an extremely controlled manner. Despite best efforts, the experiments presented in this manuscript had slight (unavoidable) differences between experimental setups for the different turret configurations. Additionally, when using a wind tunnel facility, for transonic testing it is extremely difficult to decouple the shaking associated with the fan from the shaking of specific turret components.

5. CONCLUSIONS

The aero-mechanical forcing on a hemispherical turret is undoubtedly a problem for many optical applications. The experiments discussed here sought to quantify the aero-mechanical contamination imposed onto a hemispherical turret in a parametric study. Hemispherical turrets of different protrusion distances were tested in both a wind tunnel and in-flight at varying Mach numbers and azimuthal angles. Beam jitter and accelerometer measurements were collected which sought to identify qualitative trends in mechanical contamination as a function of Mach number and turret protrusion. For both wind tunnel and in-flight measurements, the resultant rms radial jitter imposed onto the laser beams increased with Mach number, however, no discernable scaling patterns were observed. For the wind tunnel tests, the resultant rms radial jitter also generally increased with greater protrusion into the freestream flow. This trend was not observed in the data collected from in-flight testing. Ultimately, facilitating studies to isolate the aero-mechanical forcing contribution to beam distortion from facility specific distortions is challenging. The results presented here are not meant to discourage the study of how vibrational contamination reverberates into optical contamination, they are simply meant to highlight the difficulties that lay ahead for researching this problem.

ACKNOWLEDGEMENTS

This work is supported by the Air Force Research Lab, Cooperative agreement number FA9451-17-2-0088. The U.S. Government is authorized to reproduce and distribute reprints for governmental purposes notwithstanding any copyright notation thereon.

DISCLOSURES

Approved for public release; distribution is unlimited. Public Affairs release approval # AFRL-2021-2264.

REFERENCES

[1] Gordeyev S and Jumper E, "Fluid Dynamics and Aero-Optics of Turrets," *Progress in Aerospace Sciences*, 46, pp. 388-400. doi.org/10.1016/j.paerosci.2010.06.001 (2010).

[2] Vukasinovic B, Glezer A, Gordeyev S, Jumper E and Bower WW, "Flow Control for Aero-Optics Application," Experiments in Fluids, 54, 1492. doi:10.1007/s00348-013-1492-8 (2013).

[3] De Lucca N, Gordeyev S, Morrida J and Jumper EJ, "Investigation of Flow Dynamics Over Turrets with Different Spanwise Aspect Ratios Using PSP," AIAA Paper 2018-2047 (2018a).

[4] De Lucca N, “Studies of the Pressure Field and Related Beam Jitter for Hemisphere-on-Cylinder Turrets,” PhD thesis, University of Notre Dame (2015).
[5] Matthews E, Wang K, Wang M and Jumper E, “LES of an Aero-Optical Turret Flow at High Reynolds Number,” AIAA 2016-1461 (2016).
[6] Morrida, J, Gordeyev S and Jumper E, “Transonic Flow Dynamics Over a Hemisphere in Flight,” AIAA Paper 2016-1349 (2016).
[7] Porter C, Gordeyev S, Zenk M and Jumper E, “Flight measurements of the Aero-Optical Environment around a Flat-Windowed Turret,” AIAA Journal, 51(6), 1394-1403. doi.org/10.2514/1.J052067 (2013).
[8] Ladd J, Mani A and Bower W, “Validation of Aerodynamic and Optical Computations for the Unsteady Flow Field About a Hemisphere-on-Cylinder Turret,” AIAA Paper 2009-4118 (2009).
[9] Coirier WJ, Porter C, Barber J, Stutts J, Whiteley M, Goorskey D, and Drye R, “Aero-Optical Evaluation of Notional Turrets in Subsonic, Transonic and Supersonic Regimes” AIAA Paper 2014-2355 (2014)
[10] Jelic R, Sherer S and Greendyke R, “Simulation of Various Turret Configurations at Subsonic and Transonic Flight Conditions Using OVERLOW,” Journal of Aircraft 2013 50:2, 398-409. doi.org/10.2514/1.C031844 (2013).
[11] Kalensky, M., Gordeyev, S., Jumper, E.J., ”In-Flight Studies of Aero-Optical Distortions Around AAOL-BC,” AIAA Aviation, Dallas, TX, June 17-21, 2019, DOI: 10.2514/6.2019-3253.
[12] Kalensky, M., Diskin, Y., Whiteley, M.R., et al, “Turbulence Profiling Using AAOL-BC,” AIAA Sci-Tech, Orlando, FL, January 6-10, 2020, DOI: 10.2514/6.2020-0682.
[13] Kalensky, M., Wells, J., Gordeyev, S., “Image degradation due to different in-flight aero-optical environments,” Optical Engineering, DOI: 10.1117/1.OE.59.10.104104, 2020.
[14] Gordeyev, S., and Kalensky, M., “Effects of engine acoustics on aero-optical environment in subsonic flight,” AIAA Journal, 10.2514/1.J059484, 2020.